Scaling of the correlations among segment directions of a self-repelling polymer chain

1999 J. Phys. A: Math. Gen. 32 7875

(http://iopscience.iop.org/0305-4470/32/45/306)

J. Phys. A: Math. Gen. **32** (1999) 7875–7899. Printed in the UK PII: S0305-4470(99)04762-9

Scaling of the correlations among segment directions of a self-repelling polymer chain

Lothar Schäfer, Andrea Ostendorf and Johannes Hager
Fachbereich Physik der Universität Essen, 45117 Essen, Germany
E-mail: lsphy@next5.Theo-Phys.Uni-Essen.DE

Received 2 June 1999

Abstract. Segment directions in a self-repelling polymer chain are expected to show nontrivial universal long-range correlations. We verify this hypothesis to two-loop order of renormalized perturbation theory and we calculate the scaling function using the ϵ-expansion to order ϵ^2. The result is well confirmed by simulations of the Domb–Joyce model on a simple cubic lattice. Furthermore, it explains previous simulation results. Our results have consequences for the interpretation of the persistence length in screened polyelectrolytes.

1. Introduction

The conformation of an uncharged and flexible chain molecule in a good solvent shows a highly nontrivial structure. An indication of this structure is the well known power law found for the dependence of the mean-squared end-to-end distance R_e^2 of an isolated chain on the chain length n, i.e., on the number of the chain segments:

$$R_e^2(n) \sim n^{2\nu} \qquad n \to \infty. \tag{1.1}$$

The exponent ν only depends on the dimensionality d of the system and in three dimensions takes a value $\nu \approx 0.588$. The power law (1.1) indicates that the polymer configuration behaves approximately as a statistical fractal of fractal dimension $d_f = 1/\nu$. (For an introduction into the modern theory of polymer solutions we refer the reader to [1, 2].)

A characteristic feature of all fractals is the property of self-similarity. Roughly speaking, fractals look the same on any scale. For polymer chains this property shows up most directly in a study of internal correlations [3, 4]. We describe the microscopic chain configuration by the set of all bead positions $\boldsymbol{r}_j$, $j = 0, \ldots, n$, such that segment j connects bead $j-1$ to bead j. A measure of the internal correlations is the mean-squared distance among beads j_1 and j_2, $0 \leqslant j_1 < j_2 \leqslant n$:

$$R^2(j_1, j_2, n) = \langle (\boldsymbol{r}_{j_2} - \boldsymbol{r}_{j_1})^2 \rangle. \tag{1.2}$$

Here the angle brackets denote the thermodynamic average over all configurations. Self-similarity implies the scaling law

$$R^2(j_1, j_2, n) = R_e^2(j_2 - j_1)\mathcal{R}(p, q) \qquad n \to \infty \tag{1.3}$$

where the ratios

$$p = \frac{j_1}{j_2 - j_1} \qquad q = \frac{n - j_2}{j_2 - j_1} \tag{1.4}$$

0305-4470/99/457875+25$30.00

are kept fixed in taking the limit of long chains. The scaling function $\mathcal{R}(p, q)$ varies only weakly and stays close to 1 over the entire range $0 \leqslant p, q \leqslant \infty$. As a result, the mean-squared internal distance $R^2(j_1, j_2, n)$ almost coincides with the mean-squared end-to-end distance $R_e^2(j_2 - j_1)$ of a chain of length $j_2 - j_1$. This is the meaning of self-similarity in the present context.

In a good solvent the segments of the chain effectively repel each other. Then the fractal nature also enforces long-range correlations among the *directions* of the segment vectors

$$\boldsymbol{s}_j = \boldsymbol{r}_j - \boldsymbol{r}_{j-1} \qquad j = 1, \ldots, n. \tag{1.5}$$

This becomes obvious if we write the end-to-end vector as

$$\boldsymbol{r}_n - \boldsymbol{r}_0 = \sum_{j=1}^{n} \boldsymbol{s}_j \tag{1.6}$$

and use this form to calculate R_e^2:

$$\begin{aligned} R_e^2(n) &= \langle (\boldsymbol{r}_n - \boldsymbol{r}_0)^2 \rangle \\ &= \sum_{j=1}^{n} \boldsymbol{s}_j^2 + 2 \sum_{j_1 < j_2} \langle \boldsymbol{s}_{j_1} \cdot \boldsymbol{s}_{j_2} \rangle. \end{aligned} \tag{1.7}$$

The first contribution is proportional to n:

$$\sum_{j=1}^{n} \boldsymbol{s}_j^2 = \ell^2 n.$$

Here ℓ is the average segment size. If the correlations $\langle \boldsymbol{s}_{j_1} \cdot \boldsymbol{s}_{j_2} \rangle$ are of finite range along the chain

$$\langle \boldsymbol{s}_{j_1} \cdot \boldsymbol{s}_{j_2} \rangle \sim \exp[-\text{const}|j_2 - j_1|]$$

then the second term on the rhs of equation (1.7) also yields a contribution proportional to n. The resulting law $R_e^2 \sim n$ is characteristic for a chain without self-interaction, as is found in good approximation in a Θ-solvent at the Θ-temperature. In a good solvent the self-repulsion enforces the power law (1.1), $R_e^2 \sim n^{2\nu}$, $2\nu > 1$, which implies that the correlations $\langle \boldsymbol{s}_{j_1} \cdot \boldsymbol{s}_{j_2} \rangle$ must be of long range, so that the second term in equation (1.7) asymptotically dominates over the first. As the simplest hypothesis we may postulate a scaling law analogous to equation (1.3):

$$\langle \boldsymbol{s}_{j_1} \cdot \boldsymbol{s}_{j_2} \rangle = \text{const}|j_2 - j_1|^{2\nu-2} \mathcal{S}(p, q); \; |j_2 - j_1| \to \infty. \tag{1.8}$$

If we substitute this ansatz into equation (1.7) and also assume that we can approximate the chain configuration by a continuous space curve, then we find

$$\begin{aligned} \sum_{j_1 < j_2} \langle \boldsymbol{s}_{j_1} \cdot \boldsymbol{s}_{j_2} \rangle &\sim \int_0^n \mathrm{d}j_2 \int_0^{j_2} \mathrm{d}j_1 \, (j_2 - j_1)^{2\nu-2} \mathcal{S}\left(\frac{j_1}{j_2 - j_1}, \frac{n - j_2}{j_2 - j_1} \right) \\ &= n^{2\nu} \int_0^1 \mathrm{d}\bar{j}_2 \int_0^{\bar{j}_2} \mathrm{d}\bar{j}_1 \, (\bar{j}_2 - \bar{j}_1)^{2\nu-2} \mathcal{S}\left(\frac{\bar{j}_1}{\bar{j}_2 - \bar{j}_1}, \frac{1 - \bar{j}_2}{\bar{j}_2 - \bar{j}_1} \right) \end{aligned} \tag{1.9}$$

where we introduced the notation

$$\bar{j}_k = \frac{j_k}{n} \qquad k = 1, 2.$$

Provided the integral exists, this reproduces the power law (1.1). This argument can also be easily extended to show that the scaling form (1.3) of the internal distances is consistent with the ansatz (1.8).

However, the validity of the scaling hypothesis (1.8) is not obvious. We first mention a more technical point of concern. A standard tool for the calculation of scaling functions is the expansion in powers of $\epsilon = 4 - d$, i.e., in the deviation of the spatial dimensionality from the upper critical dimension $d = 4$. In four dimensions a self-repelling chain, up to logarithmic corrections, behaves as a noninteracting chain, as can be seen, for instance, from the result for the exponent ν: $2\nu = 1 + \epsilon/8 + \mathrm{O}(\epsilon^2)$. Now, integral (1.9) only exists by virtue of the relation $2\nu > 1$. In strict ϵ-expansion it therefore develops a singularity due to integration over small distances $|j_2 - j_1|$ ('ultraviolet' singularity). The argument for the validity of the scaling form, based on the result (1.9), therefore is not compatible with the ϵ-expansion. Indeed, in calculating R_e^2 we have to absorb the ultraviolet singularity of the second term in equation (1.7) into a renormalization of the first term, so that technically the separation of R_e^2 into the two terms of equation (1.7) is problematic.

As a related observation we note that equation (1.7), naively, would suggest a structure

$$R_e^2 = \mathrm{const}\, n^{2\nu} + \mathrm{const}\, n$$

to be compared with the well known correct result

$$R_e^2 \approx \mathrm{const}\, n^{2\nu} + \mathrm{const}\, n^{2\nu - \nu\omega} + \cdots$$

where ω is a new exponent. In the correct result no term proportional to n appears.

A more fundamental problem is related to the very way in which scaling laws are established. The basic tool is the renormalization group (RG), which relies on the dilation invariance of the system on macroscopic scales. To establish this invariance, we must carry through a sophisticated 'renormalized' form of a continuous chain limit. It is now well known that for a continuous chain the Boltzmann weight in function space is concentrated on functions $\boldsymbol{r}(j)$ which are continuous but not differentiable. Thus the analogue to a segment vector

$$\boldsymbol{s}_j \hat{=} \frac{\mathrm{d}\boldsymbol{r}(j)}{\mathrm{d}j}\,\mathrm{d}j$$

does not exist. This raises the delicate question whether the *correlations* $\langle \boldsymbol{s}_{j_1} \cdot \boldsymbol{s}_{j_2} \rangle$ survive the continuous chain limit. In technical terms, to establish the scaling law (1.8) we have to show that the correlation function $\langle \boldsymbol{s}_{j_1} \cdot \boldsymbol{s}_{j_2} \rangle$ is renormalizable.

In this paper we analyse this problem to the first nontrivial order (two loops). We show the renormalizability and verify the scaling form (1.8), and use the ϵ-expansion to calculate the scaling function $\mathcal{S}(p, q)$. We present results of a Monte Carlo simulation, which are in good accord with our analytical results.

This paper is organized as follows. In section 2 we define the model, and present results of unrenormalized perturbation theory for $\langle \boldsymbol{s}_{j_1} \cdot \boldsymbol{s}_{j_2} \rangle$. Analysis of the ultraviolet singularities, leading to renormalization and scaling laws, is carried out in section 3. Our result for the scaling function is discussed in section 4, and the Monte Carlo work is presented in section 5, where previous computer experiments are also considered. Section 6 contains a summary, and detailed perturbative expressions are collected in the appendix.

To finish this introduction we review the history of the problem. To our knowledge the scaling hypothesis (1.8) for $\langle \boldsymbol{s}_{j_1} \cdot \boldsymbol{s}_{j_2} \rangle$ was first presented by Domb and Hioe [5]. Guessing some ansatz for the scaling function $\mathcal{S}(p, q)$ these authors used results such as equation (1.9) to predict the swelling of the end-to-end distance, of the radius of gyration, or of internal distances. Except for that early work we are not aware of any analytical analysis. Simulation data have been published by Kremer and co-workers [6, 7] and by Forni *et al* [8]. In [6, 8] the authors are predominantly interested in the correlations among the directions of different arms in a star polymer. For a linear polymer they find contradictory results concerning the validity of the power law $\langle \boldsymbol{s}_{j_1} \cdot \boldsymbol{s}_{j_2} \rangle \sim |j_2 - j_1|^{2\nu - 2}$. The authors of [7] focus on the dependence of segment

direction correlations on the screening length in screened polyelectrolytes. Indeed, our work may have some implications for this problem, since it implies firm results for the limiting case of strong screening. We will comment on these previous simulations in section 5, showing that despite apparent contradictions all the results are well compatible with our analytical theory. We finally note that Miller [9] discussed direction correlations of segments averaged over their position on the chain as a function of their *spatial* distance. This problem is, in some sense, complementary to that treated in this work.

2. Unrenormalized perturbation theory

2.1. The model

We use the standard model of a discrete Gaussian chain with excluded volume interaction. The potential energy $\mathcal{V}$ is written as

$$\mathcal{V} = \mathcal{V}_0 + \mathcal{V}_2 \tag{2.1}$$

where $\mathcal{V}_0$ incorporates the connectivity of the chain.

$$\mathcal{V}_0 = \sum_{j=1}^{n} \frac{(\boldsymbol{r}_j - \boldsymbol{r}_{j-1})^2}{4\ell_0^2}. \tag{2.2}$$

The microscopic length ℓ_0 is proportional to the average segment size. The two-body interaction $\mathcal{V}_2$ is modelled as a pseudo-potential

$$\mathrm{e}^{-\mathcal{V}_2} = \prod_{j<j'}{}' [1 - (4\pi\ell_0^2)^{d/2}\beta_e \delta^d(\boldsymbol{r}_j - \boldsymbol{r}_{j'})] \tag{2.3}$$

where β_e is the dimensionless excluded volume constant. The product extends over all pairs of beads, and the prime indicates that in multiplying out the product we ignore all terms where some segment indices are equal. This amounts to an ultraviolet regularization. The neglected terms are of the same order as genuine many-body interactions, which are irrelevant for the present model.

We define the partition function as

$$\mathcal{Z} = \frac{(4\pi\ell_0^2)^{d/2}}{\Omega} \int \mathcal{D}[r_j] \mathrm{e}^{-\mathcal{V}} \tag{2.4}$$

where

$$\mathcal{D}[r_j] = \prod_{j=0}^{n} \frac{d^d r_j}{(4\pi\ell_0^2)^{d/2}} \tag{2.5}$$

and Ω denotes the volume of the system. The normalization factors in equations (2.4), (2.5) are chosen such that the partition function of a noninteracting ($\beta_e = 0$) chain reduces to 1 in the thermodynamic limit:

$$\mathcal{Z}_0 = \frac{(4\pi\ell_0^2)^{d/2}}{\Omega} \int \mathcal{D}[r_j] \mathrm{e}^{-\mathcal{V}_0} \overset{\Omega\to\infty}{=} 1.$$

To derive the correlations of the segment vectors we introduce a generating functional

$$\mathcal{Z}\{\boldsymbol{h}_j\} = \frac{(4\pi\ell_0^2)^{d/2}}{\Omega} \int \mathcal{D}[r_j] \mathrm{e}^{-\mathcal{V} + \sum_{j=1}^{n} \boldsymbol{h}_j \cdot \boldsymbol{s}_j} \tag{2.6}$$

where $\boldsymbol{s}_j = \boldsymbol{r}_j - \boldsymbol{r}_{j-1}$, equation (1.5). Taking derivatives with respect to $\boldsymbol{h}_j$ we then find

$$\langle \boldsymbol{s}_{j_1} \cdot \boldsymbol{s}_{j_2} \rangle = \frac{1}{\mathcal{Z}} \nabla_{h_{j_1}} \cdot \nabla_{h_{j_2}} \mathcal{Z}\{\boldsymbol{h}_j\} \Big|_{\{\boldsymbol{h}_j = 0\}}. \tag{2.7}$$

We note in passing that the generating functional $\mathcal{Z}\{\boldsymbol{h}_j\}$ for $\boldsymbol{h}_j \equiv \boldsymbol{h}$ independent of j, describes a chain under external strain, and also up to the normalization $\mathcal{Z}^{-1}$ equals the Fourier transformed end-to-end distribution for momentum $\boldsymbol{q} = \mathrm{i}\boldsymbol{h}$.

2.2. General structure of perturbation theory

For the present problem the adequate form of perturbation theory is the cluster expansion, which is based on the expansion of the product (2.3) in powers of β_e. The resulting contributions can be represented by Feynman diagrams, and here we recall the standard results [2], using the partition function (2.4) as an example. A diagram contributing to μth order (μ loops) consists of a straight line representing the polymer and μ broken lines representing the interactions. The endpoints of the broken lines are attached to the polymer line and are referred to as 'special points' in what follows. Special points of the same or different interactions are not allowed to coincide, and the endpoints $j = 0$ or $j = n$ are also considered as special points in this context. The piece of the polymer line connecting two subsequent special points is called a propagator line. The partition function is represented by the set of all diagrams which can be constructed according to these rules.

To evaluate the contribution of a diagram we label the special points by segment indices $j, j', \ldots$, and we assign internal momentum variables $\boldsymbol{k}, \boldsymbol{k}', \ldots$ to the propagator lines. Since we work in the thermodynamic limit $\Omega \to \infty$, the variables $\boldsymbol{k}, \boldsymbol{k}', \ldots$ continuously range over infinite d-dimensional momentum space. We have to respect momentum conservation at the vertices, which means that for each vertex the sum of the incoming momenta equals the sum of the outgoing momenta. (To make this precise we should assign to each propagator line some direction of momentum flow.) Then the contribution of a diagram is evaluated as follows:

(i) A broken line yields a factor of $-(4\pi\ell_0^2)^{d/2}\beta_e$, and a propagator line of momentum $\boldsymbol{k}$ connecting special points j and j', $j' > j$, stands for the propagator

$$G_0(\boldsymbol{k}, j' - j) = \mathrm{e}^{-k^2\ell_0^2(j'-j)}. \tag{2.8}$$

(ii) We integrate over all internal momenta:

$$\int \frac{d^d k}{(2\pi)^d} \ldots \equiv \int_{\boldsymbol{k}} \ldots$$

and we sum all $j, j', \ldots$ over the chain, respecting their ordering along the chain as given by the diagram. With our normalization no further factors occur.

To exemplify these rules we evaluate the partition function to first order. Figure 1 shows the diagrammatic representation. The analytic result reads

$$\mathcal{Z} = 1 - (4\pi\ell_0^2)^{d/2}\beta_e \sum_{0<j<j'<n} \int_{\boldsymbol{k}} \mathrm{e}^{-k^2\ell_0^2(j'-j)} + \mathrm{O}(\beta_e^2). \tag{2.9}$$

It is very easy to derive the corresponding rules for the generating functional $\mathcal{Z}\{\boldsymbol{h}_j\}$ (equation (2.6)). The only modification concerns the propagator, which now takes the form

$$G_0(\boldsymbol{k}, j, j', \{\boldsymbol{h}_{j''}\}) = \exp\left[-\ell_0^2 \sum_{j''=j+1}^{j'} (\boldsymbol{k} - \mathrm{i}\boldsymbol{h}_{j''})^2 \right]. \tag{2.10}$$

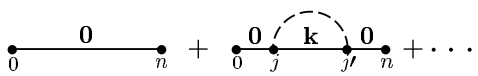

Figure 1. Diagrams for the partition function to order β_e. The special points are indicated as heavy dots.

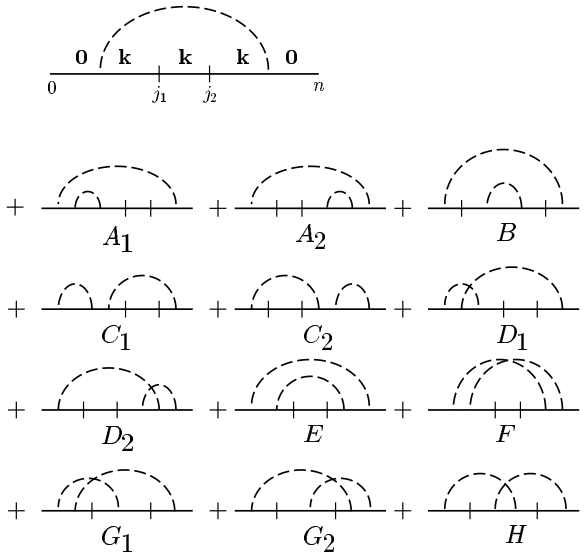

Figure 2. Diagrams of order β_e and β_e^2 contributing to $\mathcal{Z}''$.

We are interested in derivatives with respect to $\boldsymbol{h}$. Assuming $j < \hat{j} < j'$ we find

$$\nabla_{h_j} G_0(\boldsymbol{k}, j, j', \{\boldsymbol{h}_{j''}\}) = G_0(\boldsymbol{k}, j, \hat{j}, \{\boldsymbol{h}_{j''}\}) 2\mathrm{i}\ell_0^2 (\boldsymbol{k} - \mathrm{i}\boldsymbol{h}_{\hat{j}}) G_0(\boldsymbol{k}, \hat{j}, j', \{\boldsymbol{h}_{j''}\}). \tag{2.11}$$

Diagrammatically we may represent this by a vertical stroke, which introduces the new special point $\hat{j}$ (see figure 2). To the integrand this stroke contributes a factor $2\mathrm{i}\ell_0^2(\boldsymbol{k} - \mathrm{i}\boldsymbol{h}_{\hat{j}})$, where $\boldsymbol{k}$ is the momentum flowing through the special point $\hat{j}$. $\hat{j}$ is not summed over, of course. Thus

$$\mathcal{Z}'' = \nabla_{h_{j_1}} \cdot \nabla_{h_{j_2}} \mathcal{Z}\{\boldsymbol{h}_j\}|_{\{\boldsymbol{h}_j = 0\}} \tag{2.12}$$

is represented by the set of all diagrams with strokes in segments j_1, j_2. Due to $\{\boldsymbol{h}_j = 0\}$ the propagator reduces to the form (2.8).

In the evaluation of $\mathcal{Z}''$ all diagrams in which zero momentum flows through one of the points j_1, j_2 vanish trivially. By isotropy of the momentum integrations also all those diagrams vanish in which the momenta flowing through j_1 and j_2 are unrelated to each other. Physically, this amounts to the observation that for a spatial configuration of the chain that contains a loop which is closed by a pair of interacting segments and does not interact with the rest of the chain, the segment directions in the loop are independent of the configuration of the outer parts of the chain. These considerations reduce the number of diagrams to be considered. The remaining contributions up to order β_e^2 are shown in figure 2. Note that no contribution of order β_e^0 occurs, since the segment directions in a Gaussian chain are uncorrelated. Note further that diagrams (A_1, A_2) etc, are connected by reflection symmetry of the chain.

2.3. Perturbative results

In order β_e only the first diagram of figure 2 contributes. It yields

$$\begin{aligned} \mathcal{Z}'' &= -(4\pi\ell_0^2)^{d/2} \beta_e (2\mathrm{i}\ell_0^2)^2 \sum_{j=1}^{j_1-1} \sum_{j'=j_2+1}^{n-1} \int_{\boldsymbol{k}} k^2 \mathrm{e}^{-k^2\ell_0^2(j'-j)} + \mathrm{O}(\beta_e^2) \\ &= 2d\beta_e \ell_0^2 J_0 + \mathrm{O}(\beta_e^2) \end{aligned} \tag{2.13}$$

where

$$J_0 = \sum_{j=1}^{j_1-1} \sum_{j'=j_2+1}^{n-1} (j'-j)^{-1-d/2}. \tag{2.14}$$

We are interested in the limit of long chains $n \gg 1$ and also of long subchains $j_2 - j_1 \gg 1$. Then, to leading order we can evaluate the summations as integrals to find

$$\begin{aligned} J_0 &= \int_0^{j_1} \mathrm{d}j \int_{j_2}^{n} \mathrm{d}j' \, (j'-j)^{-1-d/2} \\ &= \frac{4}{d(d-2)}[(j_2-j_1)^{1-d/2} + n^{1-d/2} - (n-j_1)^{1-d/2} - j_2^{1-d/2}]. \end{aligned} \tag{2.15}$$

The corrections to this 'continuous chain limit' here are of relative order $1/(j_2 - j_1)$. The result is finite for all d, which is due to the fact that the piece $j_2 - j_1 \gg 1$ acts as an ultraviolet cut-off in the momentum integration.

To illustrate the features showing up in second order we evaluate diagram A_1. The Feynman rules yield

$$\begin{aligned} A_1 = (4\pi\ell_0^2)^d \beta_e^2 (-4\ell_0^4) \sum_{m_1=1}^{j_1-3} \sum_{m_2=j_2+1}^{n-1} \sum_{m_3=m_1+1}^{j_1-2} \sum_{m_4=m_3+1}^{j_1-1} \int_{\boldsymbol{k}_2} \mathrm{e}^{-k_2^2\ell_0^2(m_4-m_3)} \\ \times \int_{\boldsymbol{k}_1} k_1^2 \mathrm{e}^{-k_1^2\ell_0^2(m_3-m_1+m_2-m_4)} \end{aligned}$$

where we labelled the special points attached to the vertices by $m_1, \ldots, m_4$, with the ordering $m_1 < m_3 < m_4 < j_1$; $j_2 < m_2$. After momentum integration and redefinition $m_4 - m_3 \to m_4$ we can carry through the summation over m_3 to find

$$A_1 = -2d\ell_0^2\beta_e^2 \sum_{m_1=1}^{j_1-3} \sum_{m_2=j_2+1}^{n-1} \sum_{m_4=1}^{j_1-m_1-2} (j_1-1-m_4-m_1) m_4^{-d/2} (m_2-m_1-m_4)^{-1-d/2}.$$

Here the summations cannot be directly evaluated as integrals, since the m_4-integral for $d \geqslant 2$ would be singular at the lower bound $m_4 = 0$. To isolate the 'dangerous' terms we write

$$\begin{aligned} (j_1-1-m_4-m_1) m_4^{-d/2} (m_2-m_1-m_4)^{-1-d/2} &= (j_1-1-m_1)(m_2-m_1)^{-1-d/2} m_4^{-d/2} \\ &+ (j_1-1-m_1)[(m_2-m_1-m_4)^{-1-d/2} - (m_2-m_1)^{-1-d/2}] m_4^{-d/2} \\ &- m_4^{1-d/2} (m_2-m_1-m_4)^{-1-d/2}. \end{aligned}$$

Now only the first term gives rise to concern, and summing this term over m_4 we write

$$\begin{aligned} &(j_1-1-m_1)(m_2-m_1)^{-1-d/2} \sum_{m_4=1}^{j_1-m_1-2} m_4^{-d/2} \\ &\quad = (j_1-1-m_1)(m_2-m_1)^{-1-d/2} \left[\zeta\left(\frac{d}{2}\right) - \sum_{m_4=j_1-m_1-1}^{\infty} m_4^{-d/2} \right] \end{aligned}$$

where $\zeta(x)$ denotes the Riemann ζ-function. We thus find

$$A_1 = -2d\ell_0^2\beta_e^2 \sum_{m_1=1}^{j_1-3} \sum_{m_2=j_2+1}^{n-1} (j_1-1-m_1)(m_2-m_1)^{-d/2-1} \zeta\left(\frac{d}{2}\right) + \tilde{A}_1$$

where all summations in $\tilde{A}_1$ can be evaluated as integrals, convergent for $d < 4$. The final expression for $\tilde{A}_1$ is given in the appendix.

Similar expressions involving $\zeta(\frac{d}{2})$ arise from diagrams A_2 to C_2, which all involve a 'mass insertion', i.e., a nontrivial subdiagram which can be separated from the remainder of the diagram by two cuts and which does not contain an external vertex j_1 or j_2. Diagrams D_1 to H for $d < 4$ yield convergent integrals. Collecting all terms containing $\zeta(\frac{d}{2})$ we find

$$\mathcal{Z}'' = 2d\beta_e \ell_0^2 J_0 \left[1 - \beta_e \left(n\zeta\left(\frac{d}{2}\right) + \mathrm{O}(n^0)\right)\right] + \tilde{A}_1 + \cdots + \tilde{H} \tag{2.16}$$

where in the contribution proportional to $\zeta\left(\frac{d}{2}\right)$ we neglected terms of relative order $(j_2 - j_1)^{-1}$ or n^{-1}.

Now the term proportional to $\zeta\left(\frac{d}{2}\right)$ arises from the discrete microstructure of the chain. If $\langle \boldsymbol{s}_{j_1} \cdot \boldsymbol{s}_{j_2} \rangle$ gives rise to a universal, i.e. microstructure-independent result, this term must cancel against the normalizing denominator $\mathcal{Z}^{-1}$. Indeed, evaluating $\mathcal{Z}$, (equation (2.9)), along the lines sketched above, we find

$$\mathcal{Z} = 1 - \beta_e \left[n\zeta\left(\frac{d}{2}\right) - \frac{2}{\epsilon}(n^{\epsilon/2} - 1) - \frac{n^{\epsilon/2}}{1 - \epsilon/2} + \mathrm{O}(n^0)\right] + \mathrm{O}(\beta_e^2) \tag{2.17}$$

where $\epsilon = 4 - d$. Thus the terms proportional to $n\zeta(\frac{d}{2})$ cancel in the expansion of $\mathcal{Z}''/\mathcal{Z}$. The remaining terms of order n^0 could be absorbed into a redefinition of ℓ_0. However, it is more in line with the present evaluation of the diagrams to consistently take the naive continuous chain limit. This limit is defined as

$$\ell_0 \to 0$$

with

$$\tilde{\beta}_e = \ell_0^{-\epsilon} \beta_e \qquad \tilde{n} = \ell_0^2 n \qquad \tilde{j}_1 = \ell_0^2 j_1 \text{ etc} \tag{2.18}$$

kept fixed. Substituting these expressions into J_0 (equation (2.15)) we find

$$J_0 = \ell_0^{2-\epsilon} \tilde{J}_0 \tag{2.19}$$

where $\tilde{J}_0$ is given by equation (2.15) with n replaced by $\tilde{n}$, etc. The leading contribution to $\mathcal{Z}''$ takes the form

$$\mathcal{Z}'' = 2d\tilde{\beta}_e \ell_0^4 \tilde{J}_0 + \mathrm{O}(\tilde{\beta}_e^2).$$

Combining equations (2.7), (2.16)–(2.19) we find

$$\ell_0^{-4} \langle \boldsymbol{s}_{j_1} \cdot \boldsymbol{s}_{j_2} \rangle = 2d\tilde{\beta}_e \tilde{J}_0 \left[1 - \tilde{\beta}_e \tilde{n}^{\epsilon/2} \frac{4}{\epsilon(2-\epsilon)}\right] + \ell_0^{-4}[\tilde{A}_1 + \cdots + \tilde{H}] + \mathrm{O}(\ell_0^{\epsilon}) + \mathrm{O}(\tilde{\beta}_e^3). \tag{2.20}$$

Inspecting the results for $\tilde{A}_1$ to $\tilde{H}$ given in the appendix it is easily checked that the limits $\lim_{\ell_0 \to 0}(\ell_0^{-4}\tilde{A}_1)$ etc exist for $d < 4$ and yield finite functions of $\tilde{n}$, $\tilde{j}_1$, $\tilde{j}_2$. Equation (2.20) is the consistent result of unrenormalized perturbation theory in the continuous chain limit. In this derivation the cancellation of the terms $\sim n\xi\left(\frac{d}{2}\right)$ was essential. Even if we do not take the continuous chain limit this cancellation is a first hint that the segment direction correlations show some degree of universality.

3. Renormalization and scaling

3.1. Generalities

To establish universal scaling laws we have to show that the theory is renormalizable, which means that all the leading microstructure dependence can be absorbed into a redefinition of the parameters of the theory. In the more physically intuitive discrete chain model the

microstructure shows up in the dependence of the unrenormalized results on the segment size ℓ_0. Taking for $d < 4$ the naive continuous chain limit $\ell_0 \to 0$ ('dimensional regularization'), we suppress the explicit ℓ_0-dependence, and we shift the microstructure information to pole-type singularities, which show up for $\epsilon = 4 - d \to 0$. Renormalization then has to eliminate these singularities. For more detailed explanations we refer the reader to the literature [1, 2].

Following the standard route we introduce a renormalized coupling u and renormalized variables n_R, j_{1R}, j_{2R} via the formal relations

$$\tilde{\beta}_e = \ell_R^{-\epsilon} u Z_u(u) \tag{3.1i}$$

$$\tilde{n} = \ell_R^2 n_R Z_n(u) \tag{3.1ii}$$

$$\tilde{j}_k = \ell_R^2 j_{kR} Z_n(u) \qquad k = 1, 2. \tag{3.1iii}$$

The length scale ℓ_R takes care of the spatial dimensions in the renormalized theory and can be chosen arbitrarily. The renormalization factors Z_u, Z_n have to absorb the poles in ϵ (minimal subtraction). Following the conventions of [2] we use the explicit expressions

$$\begin{aligned} Z_u(u) &= \frac{1}{2}\left(1 + \frac{4}{\epsilon}u + \mathrm{O}(u^2)\right) \\ Z_n(u) &= 1 - \frac{u}{\epsilon} + \mathrm{O}(u^2). \end{aligned} \tag{3.2}$$

Using these relations to eliminate the bare parameters $\tilde{\beta}_e, \tilde{n}$, etc in favour of their renormalized counterparts u, n_R, etc for properly normalized observables such as $R^2(j_1, j_2, n)$ (equation (1.2)) we find power series in u with coefficients which for $d \leqslant 4$ are finite functions of n_R, etc. This is the statement of renormalizability, which holds to all orders of renormalized perturbation theory.

3.2. Renormalizability of direction correlations

In appendix A.2 we have given the explicit form of the singular parts of the two-loop contributions. Substituting these results into the ϵ-expanded form of equation (2.20) we find

$$\frac{1}{d}\ell_0^{-4}\langle \boldsymbol{s}_{j_1} \cdot \boldsymbol{s}_{j_2}\rangle = 2\tilde{\beta}_e \tilde{J}_0^{(0)}(1 + \mathrm{O}(\epsilon)) - \frac{12}{\epsilon}\tilde{\beta}_e^2 \tilde{J}_0^{(0)} + \mathrm{O}(\tilde{\beta}_e^2\epsilon^0, \tilde{\beta}_e^3) \tag{3.3}$$

where

$$\tilde{J}_0^{(0)} = \frac{1}{2}\left[\frac{1}{\tilde{j}_2 - \tilde{j}_1} + \frac{1}{\tilde{n}} - \frac{1}{\tilde{n} - \tilde{j}_1} - \frac{1}{\tilde{j}_2}\right] \tag{3.4}$$

(cf equation (A.17)). Here we do not write out the lengthy expression for the regular contribution in order $\tilde{\beta}_e^2$. These are given in the next section in their shortest possible form. With equations (3.1), (3.2) we find

$$\frac{1}{d}\ell_0^{-4}\langle \boldsymbol{s}_{j_1} \cdot \boldsymbol{s}_{j_2}\rangle = \ell_R^{-2} u J_{0R}\left(1 + \frac{2}{\epsilon}u\right) + \mathrm{O}(u\epsilon, u^2\epsilon^0, u^3) \tag{3.5}$$

where

$$J_{0R} = \frac{1}{2}\left(\frac{1}{j_{2R} - j_{1R}} + \frac{1}{n_R} - \frac{1}{n_R - j_{1R}} - \frac{1}{j_{2R}}\right). \tag{3.6}$$

Obviously, the simple replacement of unrenormalized by renormalized variables is not sufficient to eliminate all the divergences. In view of the sum rule (1.7) this was to be indeed expected. As is well known, R_e^2 renormalizes according to

$$R_e^2(n, \beta_e) = \ell_R^2 R_{eR}^2(n_R, u).$$

Naively renormalizing equation (1.7) we thus find

$$\ell_R^2 R_{eR}^2(n_R, u) \sim \int_0^{n_R} \mathrm{d}j_{2R} \int_0^{j_{2R}} \mathrm{d}j_{1R}\, \frac{\ell_R^4}{\ell_0^4} Z_n^2 \langle \boldsymbol{s}_{j_1} \cdot \boldsymbol{s}_{j_2} \rangle$$

where we used the replacement

$$\sum_j \to \ell_0^{-2} \int \mathrm{d}\tilde{j} \to \frac{\ell_R^2}{\ell_0^2} Z_n \int \mathrm{d}j_R.$$

This suggests defining the renormalized form of the direction correlation function as

$$\langle \boldsymbol{s}_{j_1} \cdot \boldsymbol{s}_{j_2} \rangle_R = \frac{\ell_R^2}{\ell_0^4} Z_n^2 \langle \boldsymbol{s}_{j_1} \cdot \boldsymbol{s}_{j_2} \rangle. \tag{3.7}$$

With equations (3.2), (3.5) we indeed find

$$\frac{1}{d} \langle \boldsymbol{s}_{j_1} \cdot \boldsymbol{s}_{j_2} \rangle_R = u J_{0R} + \mathrm{O}(u\epsilon, u^2, \epsilon^0, u^3) \tag{3.8}$$

a result finite for $\epsilon = 0$. This verifies the renormalizability of the segment direction correlation function to two-loop order.

3.3. RG mapping

The physical observables are the unrenormalized quantities, not their renormalized counterparts. To calculate the observables from relations such as equation (3.7) we have to know the mapping from unrenormalized to renormalized parameters, or the Z-factors, equivalently. The expansions (3.2) cannot be used directly for this purpose, since they are singular for $\epsilon = 0$, which is the remainder of a strong microstructure dependence in the discrete chain model. This problem is solved by the RG, which exploits the fact that ℓ_R is an arbitrary scale. Taking in equations (3.1) the logarithmic derivative with respect to ℓ_R, keeping all unrenormalized quantities fixed, we derive RG flow equations of the form

$$-\ell_R \frac{\mathrm{d}}{\mathrm{d}\ell_R} u = -\epsilon u + \hat{W}(u) \tag{3.9}$$

$$-\ell_R \frac{\mathrm{d}}{\mathrm{d}\ell_R} \ln Z_n = 2 - \frac{1}{\nu(u)}. \tag{3.10}$$

The functions $\hat{W}(u)$, $\nu(u)$ are known to be independent of ϵ and of microstructure effects, and can be expanded in powers of u. Furthermore, it turns out that u for $\ell_R \to \infty$ reaches a nontrivial fixed point $u^* = \mathrm{O}(\epsilon)$, which is defined as the nontrivial zero of the rhs of equation (3.9). The integrated form of the RG mapping, quite generally, can be written as

$$\ell_R = f|1-f|^{-\frac{1}{\omega}} H_u(f) s_\ell \tag{3.11i}$$

$$\ell_0^2 Z_n^{-1} = |1-f|^{\frac{1}{\omega}(\frac{1}{\nu}-2)} H(f) \tilde{\ell}^2 \tag{3.11ii}$$

where f is the renormalized coupling, normalized to u^*:

$$f = \frac{u}{u^*}. \tag{3.12}$$

The critical exponents ω, ν are defined as

$$\omega = \frac{\mathrm{d}}{\mathrm{d}u} (\hat{W}(u) - \epsilon u)|_{u=u^*}$$

$$\nu = \nu(u^*)$$

and the constants $\tilde{\ell}, s_\ell$ absorb the initial conditions needed in integrating the flow equations (3.9), (3.10). The functions $H_u(f)$ and $H(f)$ are assumed to be regular for $f \neq 0$, positive definite in the range of interest. We note that equations (3.11) involve the absolute value $|1-f|$ and thus give rise to two separate branches of the RG flow. The weak-coupling branch $0 \leqslant f < 1$ connects the Θ-point (Gaussian fixed point) $f = 0$ to the nontrivial fixed point $f = 1$. The strong-coupling branch $f > 1$ runs off to some limit which is not accessible to our perturbative theory.

The RG mapping (3.9), (3.10) and thus also the integrated form (3.11) is known most precisely from higher-order calculations, combined with Borel resummation methods [10]. In $d = 3$ the exponents take the values

$$\nu = 0.588 \qquad \omega = 0.80 \tag{3.13}$$

whereas the functions $H_u(f)$, $H(f)$ within the accuracy of the calculation can be parametrized as

$$\begin{aligned} H_u(f) &= (1 + 0.824f)^{0.25} \\ H(f) &= 1 - 0.005f - 0.028f^2 + 0.022f^3. \end{aligned} \tag{3.14}$$

The fixed-point coupling takes the value

$$u^* = 0.364.$$

For later use we also note the result of low-order ϵ-expansion:

$$u^* = \frac{\epsilon}{4} + \frac{21}{128}\epsilon^2 + \mathrm{O}(\epsilon^3). \tag{3.15}$$

In what follows we will use the high-order results (3.13), (3.14) for the RG mapping (3.11) to evaluate our results for $d = 3$, even though we have calculated the scaling functions only to two-loop order. Such a procedure involves no inconsistency since the two problems of determining the RG mapping and calculating the scaling functions are conceptually well separated. General experience shows that for quantitative calculations precise knowledge of the RG mapping is essential, whereas the scaling functions do not show much structure and can be approximated by a low-order calculation.

3.4. General scaling behaviour

The renormalized correlation function $\langle \boldsymbol{s}_{j_1} \cdot \boldsymbol{s}_{j_2} \rangle_R$ (equation (3.7)) is dimensionless and depends on the renormalized variables j_{1R}, j_{2R}, n_R, f. We may write it in the form

$$\frac{1}{d}\langle \boldsymbol{s}_{j_1} \cdot \boldsymbol{s}_{j_2} \rangle_R = \mathcal{S}_R(j_{2R} - j_{1R}, p, q, f) \tag{3.16}$$

where (cf equation (1.4))

$$p = \frac{j_{1R}}{j_{2R} - j_{1R}} \equiv \frac{j_1}{j_2 - j_1} \qquad q = \frac{n_R - j_{2R}}{j_{2R} - j_{1R}} \equiv \frac{n - j_2}{j_2 - j_1} \tag{3.17}$$

are RG-invariant combinations of segment variables.

We now exploit our freedom in choosing ℓ_R to impose the condition

$$j_{2R} - j_{1R} = 1. \tag{3.18}$$

Since to lowest order $R^2(j_1, j_2, n)$ (equation (1.2)) is found as

$$R^2(j_1, j_2, n) = 2d\ell_R^2(j_{2R} - j_{1R}) + \mathrm{O}(u)$$

this implies that we take ℓ_R^2 to be of the order of the mean-squared distance of the two segments j_1, j_2, which is the most relevant scale in our problems. Combining equation (3.18) with equation (3.1*iii*) we find

$$\ell_R^2 = \ell_0^2(j_2 - j_1)Z_n^{-1}. \tag{3.19}$$

Using equations (3.11) we can write this as

$$f^2|1-f|^{-\frac{1}{\omega\nu}}\frac{H_u^2(f)}{H(f)} = \frac{\tilde{\ell}^2}{s_\ell^2}(j_2 - j_1) \tag{3.20}$$

an equation which determines f as function of

$$\tilde{z} = \tilde{v}(j_2 - j_1)^{1/2} \tag{3.21}$$

where $\tilde{v} = \tilde{\ell}/s_\ell$.

We first consider the excluded volume limit $f \to 1$, which from equation (3.20) is attained for $j_2 - j_1 \to \infty$. Equations (3.19), (3.11) yield

$$|1-f|^{1/\omega} \sim (j_2 - j_1)^{-\nu}$$
$$\ell_R^2 \sim (j_2 - j_1)^{2\nu}$$
$$\ell_0^2 Z_n^{-1} \sim (j_2 - j_1)^{2\nu-1}.$$

Combining these results with equations (3.7), (3.16) we find

$$\langle \boldsymbol{s}_{j_1} \cdot \boldsymbol{s}_{j_2} \rangle \sim (j_2 - j_1)^{2\nu-2}\mathcal{S}^*(p,q) \tag{3.22}$$

where

$$\mathcal{S}^*(p,q) = \mathcal{S}_R(1,p,q,1). \tag{3.23}$$

This establishes the scaling behaviour (1.8) at the fixed point.

To formulate the general scaling law, which is valid also outside the excluded volume limit, it is useful to construct a quantity in which the explicit factors of ℓ_R^2, Z_n/ℓ_0^2 occurring in equation (3.7) drop out. Z_n/ℓ_0^2 can be eliminated with the help of equation (3.19). The remaining factors of ℓ_R^2 can be expressed in terms of the end-to-end distance of a chain of length $j_2 - j_1$, which by virtue of the condition $j_{2R} - j_{1R} = 1$ takes the form

$$R_e^2(j_2 - j_1) = 2d\ell_R^2\mathcal{R}_{eR}^2(f). \tag{3.24}$$

As a result we find

$$\frac{(j_2 - j_1)^2}{R_e^2(j_2 - j_1)}\langle \boldsymbol{s}_{j_1} \cdot \boldsymbol{s}_{j_2} \rangle = \tilde{\mathcal{S}}(p,q,\tilde{z}) \tag{3.25}$$

where

$$\tilde{\mathcal{S}}(p,q,\tilde{z}) = \frac{1}{2}\frac{\mathcal{S}_R(p,q,f(\tilde{z}))}{\mathcal{R}_{eR}^2(f(\tilde{z}))} \tag{3.26}$$

is a universal scaling function. The only microstructure-dependent parameter left is the scale $\tilde{v}$ occurring in $\tilde{z}$ (equation (3.21)). We recall that the function $f(\tilde{z})$, which is defined as the solution of equation (3.20), shows two branches, depending on $f \lessgtr 1$. Therefore, $\tilde{\mathcal{S}}(p,q,\tilde{z})$ also shows a two-branch structure. We furthermore note that in the excluded volume limit $\tilde{z} \to \infty$, i.e. $f \to 1$, $\tilde{\mathcal{S}}(p,q,\infty)$ becomes fully universal, independent of any microscopic parameters.

4. Quantitative results for the scaling function

Evaluating the integrals of appendix A.1 and using the well known [2] result $\mathcal{R}^2_{eR}(f) = 1 - \frac{\epsilon}{8} f + \mathrm{O}(\epsilon^2)$ we have calculated the scaling function $\tilde{\mathcal{S}}(p, q, \tilde{z})$ to second order of the ϵ-expansion. As is well known the quantitative results depend somewhat on the precise choice of the quantities to expand. In the present case the scaling function $\tilde{\mathcal{S}}$ contains a prefactor of $u = u^* f$, and the result weakly depends on whether we use the strict ϵ-expansion (3.15) for u^* or keep the prefactor u^*, taking $u^* = 0.364$ in the evaluation in $d = 3$. To isolate this ambiguity of the overall amplitude we write

$$\tilde{\mathcal{S}}(p, q, \tilde{z}) = \tilde{\mathcal{S}}_\infty(\tilde{z}) \bar{\mathcal{S}}(p, q, \tilde{z}) \tag{4.1}$$

where

$$\tilde{\mathcal{S}}_\infty(\tilde{z}) = \tilde{\mathcal{S}}(\infty, \infty, \tilde{z}) \tag{4.2}$$

absorbs the prefactor of u^*. Here we assumed that the segment direction correlations in the interior of an infinitely long chain ($p \to \infty, q \to \infty$) take a well defined limit. This is verified by our ϵ-expansion results.

The amplitude $\tilde{\mathcal{S}}_\infty(\tilde{z})$ is found as

$$\tilde{\mathcal{S}}_\infty(\tilde{z}) = \tfrac{1}{4} u^* f (1 + \tfrac{3}{4}\epsilon - \tfrac{5}{8}\epsilon f + \mathrm{O}(\epsilon^2)) \tag{4.3i}$$

with the strict ϵ-expansion taking the form (cf equation (3.15))

$$\tilde{\mathcal{S}}_\infty(\tilde{z}) = \frac{\epsilon}{16} f \left(1 + \frac{45}{32}\epsilon - \frac{5}{8}\epsilon f + \mathrm{O}(\epsilon^2)\right). \tag{4.3ii}$$

At the fixed point $f = 1$ and for three dimensions ($\epsilon = 1$) the strict ϵ-expansion (4.3ii) yields $\tilde{\mathcal{S}}_\infty(\tilde{z} \to \infty) = 0.111$, whereas the form (4.3$i$), evaluated with $u^* = 0.364$, yields $\tilde{\mathcal{S}}_\infty(\tilde{z} \to \infty) = 0.102$. We thus find an ambiguity of the order of 10% in the overall amplitude $\tilde{\mathcal{S}}_\infty$. This ambiguity is not too large in view of the sizeable correction of order ϵ^2. Note that for $f = 1$ equation (4.3ii) yields

$$\tilde{\mathcal{S}}_\infty(\tilde{z}) = \frac{\epsilon}{16}\left(1 + \frac{25}{32}\epsilon + \mathrm{O}(\epsilon^2)\right)$$

so that for $\epsilon = 1$ the $\mathrm{O}(\epsilon^2)$ contribution almost doubles this universal ratio. We note further that a similar behaviour is observed for the interpenetration ratio ψ^*, which also is proportional to u^*.

Being normalized to $\bar{\mathcal{S}}(\infty, \infty, \tilde{z}) = 1$, the function $\bar{\mathcal{S}}(p, q, \tilde{z})$ does not suffer from the ambiguities of the overall amplitude $\tilde{\mathcal{S}}_\infty$. Our full ϵ-expansion result is lengthy:

$$\begin{aligned}\bar{\mathcal{S}}(p, q, \tilde{z}) = 1 &+ \frac{1}{1+p+q} - \frac{1}{1+q} - \frac{1}{1+p} + \frac{\epsilon}{2}\left[\frac{\ln(1+p+q)}{1+p+q} - \frac{\ln(1+q)}{1+q} - \frac{\ln(1+p)}{1+p}\right] \\ &+ \frac{\epsilon}{8} f [g(p, q) + g(q, p)]\end{aligned} \tag{4.4}$$

where

$$\begin{aligned}g(p, q) = &\frac{1}{2(1+p+q)} - \frac{1}{2(1+p)} \\ &- \left(1 + \frac{1}{4p} - \frac{4}{1+p} + \frac{2}{(1+p)^2} + \frac{1}{2(1+q)} + \frac{3}{4(1+p+q)}\right)\ln p \\ &+ \left(\frac{5}{2(1+p)} + \frac{1}{4q} + \frac{3}{4(1+p+q)}\right)\ln(1+p)\end{aligned}$$

$$+\left(\frac{1}{1+p}-\frac{3}{2(1+p+q)}-\frac{1}{2}\right)\ln(1+p+q)$$
$$+\frac{1}{2}\left(1-\frac{3}{1+p+q}+\frac{2}{(1+p+q)^2}\right)\ln(p+q)+\frac{1}{4}\left(1+\frac{1}{p}\right)\ln(p+q+pq)$$
$$+\frac{w_1(p,q)}{2(1+q)(1+p+q)}\ln\frac{w_1(p,q)-p}{w_1(p,q)+p}-\frac{w_2(p)}{2(1+p)}\ln\frac{w_2(p)-p}{w_2(p)+p}$$
$$+\frac{w_3(p,q)}{2(1+p)(1+p+q)}\ln\frac{1+p+2q-w_3(p,q)}{1+p+2q+w_3(p,q)}$$
$$+\frac{w_3(p,q)}{4q(1+p+q)}\ln\frac{(1+p)(p+2q)-pw_3(p,q)}{(1+p)(p+2q)+pw_3(p,q)}$$
$$-\frac{w_4(p)}{2(1+p)}\ln\frac{1+2p-w_4(p)}{1+2p+w_4(p)} \tag{4.5}$$

$$w_1(p,q)=p^{1/2}(4+p+4q)^{1/2} \tag{4.6}$$
$$w_2(p)=p^{1/2}(4+p)^{1/2} \tag{4.7}$$
$$w_3(p,q)=(1+p)^{1/2}(1+p+4q)^{1/2} \tag{4.8}$$
$$w_4(p)=(1+4p)^{1/2}. \tag{4.9}$$

We now consider this result in various limits.

(i) Segments j_1, j_2 well inside an infinitely long chain:

$$p=x\alpha \qquad q=\frac{x}{\alpha} \qquad x\to\infty \qquad 0<\alpha<\infty.$$

We find

$$\bar{\mathcal{S}}(p,q,\tilde{z})=1+\frac{1}{x}\left(\frac{\alpha}{1+\alpha^2}-\frac{1}{\alpha}-\alpha\right)$$
$$+\frac{\epsilon}{2}\frac{\ln x}{x}\left[\frac{\alpha}{1+\alpha^2}-\frac{1}{\alpha}-\alpha+f\left(\frac{2}{\alpha}+2\alpha-\frac{3\alpha}{2(1+\alpha^2)}\right)\right]+\epsilon\mathrm{O}\left(\frac{1}{x}\right)$$
$$+\mathrm{O}(\epsilon^2). \tag{4.10}$$

For $x\to\infty$, implying $p=j_1/(j_2-j_1)\to\infty$, $q=(n-j_2)/(j_2-j_1)\to\infty$, the influence of the end pieces j_1-0, $n-j_2$ vanishes, as expected. The approach to that limit, however, is not trivial. The term $\ln x/x$ signals the existence of an anomalous power law $\bar{\mathcal{S}}-1\sim x^{-1+\mathrm{O}(\epsilon)}$, valid in the excluded volume limit $f=1$. However, without further independent information on the exponent or on the general structure of the scaling function in the limit $p,q\to\infty$, an exponentiation of the ϵ-expansion is ambiguous. From the structure of equation (4.10) we can only say that there are at least two powers of the form $x^{-1+\mathrm{O}(\epsilon)}$, but we cannot even deduce the sign of the leading terms. Below we will find similar logarithms indicating anomalous power laws in the other limits considered. Note that the corresponding feature is observed [4] for the internal distances $R^2(j_1,j_2,n)$, defined in equation (1.2).

(ii) One segment approaches a chain end:

$$p\to 0 \qquad q \text{ fixed.}$$

We find

$$\bar{\mathcal{S}}(p,q,\tilde{z})=\left(1-\frac{1}{(1+q)^2}\right)p\left(1-\frac{\epsilon}{8}f\ln p\right)+\epsilon\mathrm{O}(p)+\mathrm{O}(\epsilon^2). \tag{4.11}$$

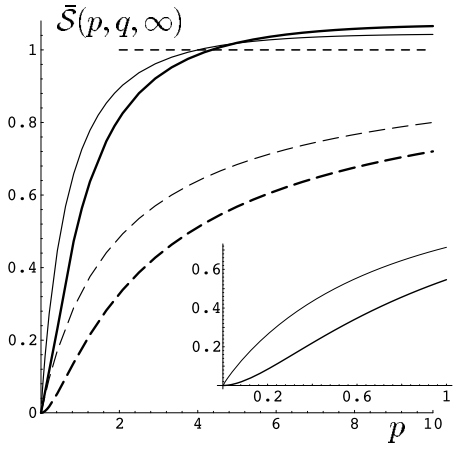

Figure 3. Normalized scaling function $\bar{\mathcal{S}}(p,q,\tilde{z})$ in the excluded volume limit $\tilde{z}=\infty$. Full curves: two-loop results; broken curves: one-loop results. Thick lines: $q=p$, thin curves: $q=\infty$. The inset magnifies the small p behaviour.

Thus the segment direction correlation function vanishes as $p^{1+\mathrm{O}(\epsilon)}$, which implies that towards the chain ends the segments rapidly forget about the direction of the segments in the interior of the chain. It is the strain exerted by the end pieces, that leads to the direction correlations. This is already obvious from the leading-order diagram in figure 2, which suppresses configurations where the end pieces are close together.

(iii) The interior piece $(j_1,\, j_2)$ approaches the total chain, i.e. $j_1 \to 0$, $j_2 \to n$:

$$p = x\alpha \qquad q = \frac{x}{\alpha} \qquad x \to 0 \qquad 0 < \alpha < \infty.$$

We find

$$\bar{\mathcal{S}}(p,q,\tilde{z}) = 2x^2 - \frac{\epsilon}{8} f x^2 \ln x + \epsilon \mathrm{O}(x^2) + \mathrm{O}(\epsilon^2) \tag{4.12}$$

where α drops out in the explicitly given terms. As expected, $\bar{\mathcal{S}}$ vanishes more rapidly than in case (ii): $\bar{\mathcal{S}} \sim x^{2+\mathrm{O}(\epsilon)}$.

These results show that the segment direction correlations sensitively depend not only on the distance along the chain $(j_2 - j_1)$ of the two segments, but also on their precise position on the chain. This is illustrated quantitatively in figure 3, where we plot $\bar{\mathcal{S}}(p,\infty,\infty)$ and $\bar{\mathcal{S}}(p,\,p,\infty)$ as function of p. We observe that in lowest-order approximation $(\mathrm{O}(\epsilon))$ the curves approach the limiting value $\bar{\mathcal{S}}(\infty,\infty,\infty) = 1$ quite slowly from below, being governed by terms such as $1/(1+p)$ (cf equation (4.4)). The first correction $(\mathrm{O}(\epsilon^2))$, however, again makes a large effect. It considerably reduces the range, where end effects are important, so that the curves approach the limiting region $\bar{\mathcal{S}} \approx 1$ much more rapidly. Furthermore, the curves asymptotically tend to the limit $\bar{\mathcal{S}} = 1$ from above, a behaviour setting in very slowly for values of p much larger than those shown in figure 3. However, even in the $\mathrm{O}(\epsilon^2)$-approximation there is a pronounced variation of $\bar{\mathcal{S}}$ in the range $p \lesssim 5$, which is an important part of the range accessible to present day computer experiments.

To avoid all misunderstanding we should stress that our result does not imply that $\langle \boldsymbol{s}_{j_1} \cdot \boldsymbol{s}_{j_2} \rangle$ increases as function of $j_2 - j_1$. Rather, this correlation function always decreases, due to the prefactor $(j_2 - j_1)^{2\nu-2}$. It is only the ratio $\tilde{\mathcal{S}}$ (equation (3.25)), or $\bar{\mathcal{S}}$, equivalently, that increases or even overshoots for $p \to \infty, q \to \infty$. The overshooting is also seen in the analytical result (4.10), which for $p = q$, i.e. $\alpha = 1$, yields

$$\bar{\mathcal{S}}(p,\,p,\tilde{z}) = 1 - \frac{3}{2p} + \frac{\epsilon}{2}\left(-\frac{3}{2} + \frac{13}{4} f\right)\frac{\ln p}{p}.$$

Table 1. Sample size in the simulations.

w	Number of started tours	Number of tours reaching $N_{\max} = 1000$
0.095	10^8	9939 518
0.4	10^8	1165 995
1.0	10^8	221 382

For $p \to \infty$ the $\ln p/p$ term dominates, and its coefficient is positive for $f \approx 1$. Clearly, higher-order calculations will modify this result, and since the exact asymptotic structure is unknown it is not clear whether this overshooting is a valid feature. As pointed out in the context of equation (4.10) above, the ϵ-expansion result would also be perfectly consistent with an exact expression which shows no overshooting.

We close this section by making some remark on the role of the ϵ-expansion. For other quantities we can often get equally good or even superior results for the scaling functions by evaluating the renormalized perturbation theory directly in $d = 3$, avoiding the ϵ-expansion altogether. For quantities involving several scales this method works, provided only one of the scales shows critical behaviour associated with some anomalous exponent. The other scales must be 'trivial', allowing for a perturbative treatment in all limits of interest. (See [2] for an more extensive discussion.) The direction correlations involve three scales, namely $R_e^2(j_2-j_1)$, $R_e^2(j_1)$, $R_e^2(n-j_2)$, and, as found above, in limits such as $R_e^2(j_1)/R_e^2(j_2-j_1) \to 0$, corresponding to $p \to 0$, there exist new power laws with unknown exponents. Such limits would then be clearly mistreated by direct evaluation of the diagrams in $d = 3$. Furthermore, it is found here that the limit $p \to \infty, q \to \infty$, if evaluated directly in $d = 3$, induces new logarithmic singularities $\sim \ln p$ within the renormalized theory. These singularities are specific for $d = 3$. For these reasons we here consistently stay within the ϵ-expansion, using also the ϵ-expanded form (4.3*ii*) of $\tilde{\mathcal{S}}_\infty$.

5. Comparison with Monte Carlo results

5.1. Simulation method

We measured the direction correlations in the Domb–Joyce model of a polymer chain. The chain is modelled as a random walk on a cubic lattice, and each configuration is weighted by a factor $(1-w)^{n_2}/\mathcal{Z}$, where n_2 is the number of pairwise intersections and $\mathcal{Z}$ is the partition function. A multiple intersection of order m is counted as $m(m-1)/2$ pair intersections. We employed the PERM-algorithm developed by Grassberger [11] but in a slightly simplified form that employs pruned enriched simple sampling. The algorithm essentially performs a random walk in the space of chain lengths between the reflecting boundaries 0 and $N_{\max}$ and thereby samples data for all chain lengths in the interval $[0, N_{\max}]$. The bunch of data accumulated between starting from zero and reaching zero again (called tour) is highly correlated, but different tours are uncorrelated. We therefore measure the sample quality in numbers of tours rather than in numbers of walks.

For the values of w, which we employed in our simulations, the characteristics of the samples are given in table 1.

We use three different values of w.

$w = 1$**:** self-avoiding walks. In this situation we are on the strong coupling branch $f > 1$.

$w = 0.4$**:** this value is known to be on the weak coupling branch, but very close to the excluded volume limit $f = 1$. For the Domb–Joyce model the fixed point value w^* of the bare

Table 2. Fit parameter $\tilde{v}$ and resulting renormalized couplings.

w	1	0.4	0.095
$\tilde{v}$	1.74	22.04	0.29
$f(j_2 - j_1 = 11)$	1.29	0.98	0.46
$f(j_2 - j_1 = 101)$	1.085	0.993	0.705

coupling w is known [12] to be in the interval $0.4 < w^* < 0.5$.

$w = 0.095$**:** this value is deep on the weak coupling branch $f < 1$.

We first considered subchains of lengths $j_2 - j_1 = 11$ or $j_2 - j_1 = 101$, embedded as central parts into chains of lengths $n \leqslant 1000$, and we measured $\langle \boldsymbol{s}_{j_1} \cdot \boldsymbol{s}_{j_2} \rangle$ as function of $q = p = j_1/(j_2 - j_1)$ as well as $R_e^2(j_2 - j_1)$, so as to be able to construct the scaling function $\tilde{\mathcal{S}}(p, q, \tilde{z})$ (equation (3.25)). The resulting data for $\langle \boldsymbol{s}_{j_1} \cdot \boldsymbol{s}_{j_2} \rangle$ scattered strongly and therefore, in a new experiment we averaged the data over small intervals of $(j_2 - j_1)$. Specifically, '$j_2 - j_1 = 11$' in what follows stands for $j_2 - j_1 \in \{10, 11, 12\}$, whereas '$j_2 - j_1 = 101$' means $j_2 - j_1 \in \{91, \ldots, 111\}$. This averaging induces a small systematic shift of the data, which can be estimated with the help of the theoretical scaling function. It is found to be much smaller than the residual scatter of the data, and this finding is confirmed by comparing the old and the new runs. The maximal values of $q = p = j_1/(j_2 - j_1)$ reached in our simulations are $p = 44.91(j_2 - j_1 = 11)$ and $p = 4.40(j_2 - j_1 = 101)$, respectively.

5.2. Analysis of our results

We compare our numerical results with the scaling function $\tilde{\mathcal{S}}$, evaluated in the form (4.1): $\tilde{\mathcal{S}} = \tilde{\mathcal{S}}_\infty \cdot \bar{\mathcal{S}}$, with $\tilde{\mathcal{S}}_\infty$ calculated in strict ϵ-expansion (4.3*ii*). The only remaining nonuniversal parameter is the combination $\tilde{v} = \tilde{\ell}/s_\ell$, which determines $\tilde{z}$ according to equation (3.21):

$$\tilde{z} = \tilde{v}(j_2 - j_1)^{1/2}.$$

In turn, $\tilde{z}$ determines the renormalized coupling parameter f according to equation (3.20). In previous work using the Domb–Joyce model [12] we have determined the parameter $\tilde{v} = \tilde{v}(w)$ by analysing crossover results for quantities such as the end-to-end distance or the radius of gyration. However, in that work we calculated the scaling functions by renormalized perturbation theory evaluated directly in three dimensions, not using the ϵ-expansion. The choice of the renormalized theory, in the present case given by equation (3.18): $j_{2R} - j_{1R} = 1$, was optimized for such a calculation, which yields a condition that differs from equation (3.18) by a numerical factor. This in turn influences $\tilde{v}$, which thus depends both on the bare coupling w and on the precise form of the renormalized theory. Here we therefore had to carry through a new fit. We determined good values of f from the data for $j_2 - j_1 = 11$, and used these values to calculate $\tilde{v}$ according to equations (3.20), (3.21). We then used these values $\tilde{v}$ to calculate f for $j_2 - j_1 = 101$. The results are presented in table 2. We note that the resulting values of f for weak coupling ($f < 1$) are very close to the values resulting from the theory evaluated directly in $d = 3$. Only for strong coupling is the difference of the order of 10%, which signals that we approach a region where low-order perturbation theory breaks down.

Using these parameter values we have evaluated $\tilde{\mathcal{S}}(p, p, \tilde{z})$, calculated to order ϵ^2. The results are compared with our Monte Carlo data in figure 4. Clearly, the agreement is very good, in particular for weak coupling $w_0 = 0.095$. For strong coupling for $j_2 - j_1 = 11, (j_2 - j_1)/n \gtrsim 0.3$ we see deviations which might be due to 'irrelevant' $1/(j_2 - j_1)$-corrections. More significant is the observation that the data show no indication

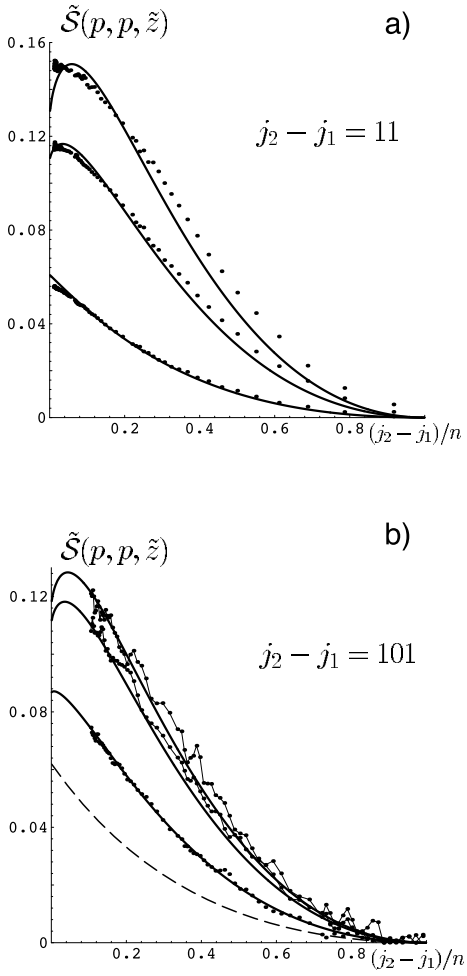

Figure 4. Scaling functions $\tilde{S}(p, p, \tilde{z})$ evaluated to order ϵ^2 as function of $(j_2 - j_1)/n = 1/(1+2p)$, compared with Monte Carlo data: (*a*) $j_2 - j_1 = 11$, (*b*) $j_2 - j_1 = 101$. The full curves and data are for $w_0 = 0.095, 0.4, 1$ from below. In (*b*) we included the order ϵ result for $w_0 = 0.4$ (broken curve), and for $w_0 = 0.4$ or 1 we connected the data points as a guide to the eye.

of overshooting for $(j_2 - j_1)/n \to 0$, i.e. $p = q \to \infty$. As we have pointed out above, the overshooting of the theoretical scaling function may be an artifact of the ϵ-expansion. To appreciate the role of the $O(\epsilon^2)$-correction we recall that the lowest-order approximation, $O(\epsilon)$, would be too small by a factor of about 2, as is clear from figure 3. In figure 4(*b*) we illustrated this by including the $O(\epsilon)$-result for $w = 0.4$. Keeping this in mind, we find the agreement among the $O(\epsilon^2)$-theory and the data truly remarkable.

5.3. Consideration of previous simulation data

Batoulis and Kremer [6] measured direction correlations in self-avoiding chains on a fcc lattice, for chain lengths $n = 60$ or 240. Forni *et al* [8] carried through an off-lattice simulation for chains of lengths $n = 472$ or 80, interacting via a Lennard-Jones potential. In both simulations one segment index (j_2) was kept fixed and the other (j_1) was varied, for the shorter chains coming close to the chain end. Thus in these simulations our parameter $p = j_1/(j_2 - j_1)$ varies, approaching zero for the shorter chains. For the longer chains the minimal value of p is $p \approx 3$ [6] or $p \approx 4$ [8], respectively. Even if we follow the authors in assuming that the systems are close to the excluded volume limit, we conclude that effective exponents

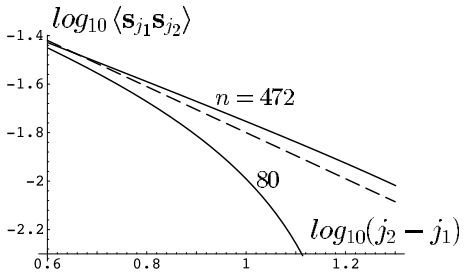

Figure 5. $\log_{10}\langle \boldsymbol{s}_{j_1} \cdot \boldsymbol{s}_{j_2}\rangle$ as a function of $\log_{10}(j_2 - j_1)$, for $n = 472$ or 80, respectively. The excluded volume limit $\tilde{z} \to \infty$ (i.e. $f = 1$) has been taken. The broken line has slope -0.95.

extracted from the data result from the superposition of the power law prefactor $(j_2 - j_1)^{2\nu-2}$ and the variation of the scaling function $\tilde{\mathcal{S}}(p, q, \tilde{z})$. As is clear from figure 3, in the range covered by the experiment the variation of $\tilde{\mathcal{S}}$ cannot be neglected, and since for fixed $j_2 > j_1$, $p = j_1/(j_2 - j_1)$ decreases with increasing $(j_2 - j_1)$, it will lead to an effective exponent μ,

$$\langle \boldsymbol{s}_{j_1} \cdot \boldsymbol{s}_{j_2}\rangle \sim (j_2 - j_1)^{-\mu}$$

which is larger than the theoretical value $2 - 2\nu = 0.824$. This is indeed found, the values quoted being $\mu = 1.15$ [6] or $\mu = 0.95$ [8], respectively.

Since the values of $j_2 - j_1$ reached by the experiments are quite small, $1 < j_2 - j_1 \lesssim 30$ or $1 < j_2 - j_1 \lesssim 20$, respectively, a precise quantitative analysis of the data does not seem appropriate. Using the values of n, j_2, j_1 of these experiments we however have plotted

$$\log_{10}\langle \boldsymbol{s}_{j_1} \cdot \boldsymbol{s}_{j_2}\rangle \sim (2\nu - 2)\log_{10}(j_2 - j_1) + \log_{10}\tilde{\mathcal{S}}$$

as a function of $\log_{10}(j_2 - j_1)$. Figure 5 shows the results for the experiment of [8], in the range $4 \leqslant j_2 - j_1 \leqslant 13$ ($n = 80$) or $4 \leqslant j_2 - j_1 \leqslant 20$ ($n = 472$). Also given is a line indicating an effective exponent of $\mu = 0.95$. This figure should be compared with the corresponding part of figure 4 in [8]. The close similarity clearly shows that the data are consistent with our theory. Carrying through the same analysis with values n, j_2, j_1 taken from [6], we find a quite similar picture, but with an effective exponent $\mu \approx 1.0$–1.1 extracted for the longer chains. Within the uncertainties of the data this is quite consistent with $\mu = 1.15$ quoted by the authors (see also the footnote in [8]). The data for the shorter chain, however, do not show the strong decrease expected for $j_1 \to 0$, which was verified in our simulations and was also found in [8]. We are unable to comment on this.

We finally consider some data of Micka and Kremer [7], which are taken for an off-lattice bead-and-spring chain, interacting via a Debye–Hückel potential. The range of the potential was varied from a strongly screened to an essentially Coulomb-like interaction, for chain lengths up to $n \approx 256$. Among the measured quantities are the direction correlations, plotted as $\ln\langle \boldsymbol{s}_{j_1} \cdot \boldsymbol{s}_{j_2}\rangle$ against $(j_2 - j_1)$. The rationale behind this semilogarithmic plot is the standard assumption that in a polyelectrolyte the direction correlations behave as in a wormlike chain:

$$\langle \boldsymbol{s}_{j_1} \cdot \boldsymbol{s}_{j_2}\rangle \sim \mathrm{e}^{-\ell(j_2 - j_1)/L_p} \tag{5.1}$$

where L_p is the persistence length. A straight portion in such plots therefore allows one to extract L_p. We should immediately note that such an ansatz, if at all valid, for a screened potential can hold only in some intermediate range of n, since the chain for any nonvanishing amount of screening in the limit $n \to \infty$ is expected to reach the excluded volume limit as described in this paper. The concept of a finite persistence length breaks down, the observed power law decay of $\langle \boldsymbol{s}_{j_1} \cdot \boldsymbol{s}_{j_2}\rangle$ essentially corresponding to $L_p \to \infty$.

In figure 6 we have plotted $\ln\langle \boldsymbol{s}_{j_1} \cdot \boldsymbol{s}_{j_2}\rangle$ as function of $j_2 - j_1$ for the central piece of the chain, assuming to be in the excluded volume limit. To make a link with the work of [7] we used values of $n = 128, 256$, but we should immediately note that this plot is somewhat

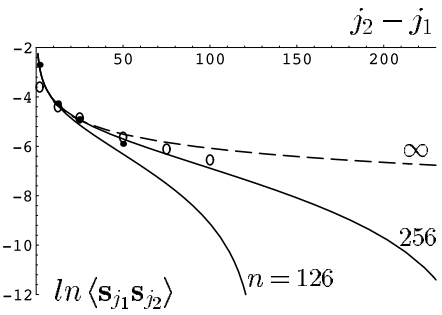

Figure 6. $\ln\langle \boldsymbol{s}_{j_1} \cdot \boldsymbol{s}_{j_2}\rangle$ as a function of $j_2 - j_1$ (excluded volume limit), evaluated for $n = 128, 256$ (full curves). The broken curve gives the infinite chain limit. The 'data points' are for $N = 256$, Debye screening parameter $\kappa = 0.48$ (dots), $\kappa = 0.16$ (circles). These points are taken from figure 1.18 of [13], with a nonuniversal vertical shift included.

redundant: the scaling law (3.22) shows that the quantity plotted is in fact a universal function of $(j_2 - j_1)/n$, up to a nonuniversal microstructure-dependent shift. On inspecting figure 6 the most important observation is that the asymptotic power law and the finite chain effects conspire to produce almost-straight intermediate parts of the curves. Following the procedure of [7], from this part we could extract a 'persistence length' $L_{p,\mathrm{eff}}$, which here would be a fairly meaningless effective quantity. However, it is also important to note that for a given chain length the resulting values of $L_{p,\mathrm{eff}}$ are bounded from above by the average slope of the asymptote $n \to \infty$ in the appropriate range of $j_2 - j_1$. The observation of larger values of $L_{p,\mathrm{eff}}$ then indicates significant effects of the larger range of the potential, which in the terminology of the present theory would be called nonuniversal 'microstructure' effects.

For the largest values of the screening parameter κ, namely $\kappa = 0.48, 0.16$, the work of [7] is clearly in the range where the effective persistence length should not be interpreted in terms of polyelectrolyte theories. To illustrate this, in figure 6 we included some averaged data points, extracted from figure 1.18 of [13], where a more extensive compilation of the data is given. This shall only demonstrate that the observed slope is well in the range predicted by excluded-volume theory. A more detailed evaluation of the data is not feasible, since clearly for fixed n the renormalized coupling f will be κ-dependent, which makes any further analysis along the lines followed here quite ambiguous.

Data for smaller screening parameters $\kappa \leqslant 0.04$ can be found in [7, 13]. These clearly show the influence of the larger range of the potential. The effective persistence length exceeds the limit set by the present theory. It is clear, however, that simple theories of the screening dependence of the persistence length can only be valid if L_p is large compared with $L_{p,\mathrm{eff}}$ as extracted from the present theory in the range of chain lengths considered. In analysing such problems the results of standard excluded volume theory should always be kept in mind.

6. Conclusions

If direction correlations among segments j_1 and j_2 can be defined in the renormalized theory and turn out to be multiplicatively renormalizable, then they obey scaling with the asymptotic power law behaviour $\sim(j_2 - j_1)^{2\nu-2}$. This is guaranteed by the sum rule relating the direction correlations to the end-to-end distance. We have verified the multiplicative renormalizability to two-loop order, which strongly supports the validity of the scaling law. Furthermore, we have constructed a crossover scaling function, which at the fixed point is independent of any microstructure parameters.

Calculating this function to order ϵ^2 we find a strong variation of the correlations with the position on the chain of the segments considered. If both end pieces $(0, j_1)$, (j_2, n) of the chain become infinitely long, then the scaling function saturates. However, it vanishes with

vanishing length of some end piece: the endsegments hold no information on the segment directions deeper inside the chain. This strong position dependence persists up to lengths of the end pieces of order $5(j_2 - j_1)$. Therefore, with present day facilities, any attempt to check the asymptotic power law $\sim(j_2 - j_1)^{2\nu-2}$ in a computer experiment must take care of the variation of the scaling function. Inspecting published data we have shown that the numerically found effective exponents are consistently explained by the theory. They result from the superposition of the asymptotic power law with the variation of the scaling function.

The new simulations presented in this work are not aimed at checking the power law but the scaling function. Since we measure effects which are small on the scale set by the segment size ℓ, the data scatter considerably. Nevertheless, we can state very good agreement with the theory. This is the more surprising since the $O(\epsilon^2)$-correction is large. Theory and experiment fit together only if we include the $O(\epsilon^2)$-terms.

Our results have consequences for an analysis of the persistence length, which is commonly defined not by the exponential law (5.1), but by the projection of the end-to-end vector on some segment direction:

$$L_p(j) = \frac{1}{\ell}\langle \boldsymbol{s}_j \cdot (\boldsymbol{r}_n - \boldsymbol{r}_0)\rangle.$$

Usually the direction of the first segment $j = 1$ is taken, and our analysis immediately shows that $L_p(1)$ in three dimensions should be of microscopic size. (In two dimensions $L_p(1)$ is less trivial, see [14].) For $j = \frac{n}{2}$, however, $L_p(\frac{n}{2})$ is expected to diverge in the limit of long chains, $n \to \infty : L_p(\frac{n}{2}) \sim n^{2\nu-1} \approx n^{0.176}$ $(d = 3)$. This immediately follows from a sum rule analogous to equation (1.7). Furthermore, we have found that from some intermediate range of the direction correlation function we may extract an effective persistence length (equation (5.1)), which, however, has no fundamental meaning. All this discussion shows that the concept of a persistence length, which is widely used in the theory of polyelectrolytes, is quite delicate. A more detailed analysis of $L_p(j)$ in the framework of excluded volume theory is currently underway.

Acknowledgments

We thank Professor Grassberger for helpful discussions. This work has been supported by the Deutsche Forschungsgemeinschaft, SFB Unordnung und grosse Fluktuationen.

Appendix

A.1. Unrenormalized two-loop contributions

Where necessary, we extract additive contributions $\sim \xi(\frac{d}{2})$, and we evaluate the remainder as integrals for general d, $2 < d < 4$. The leading corrections are then of relative order $n^{-\epsilon/2}$, transforming into $\tilde{n}^{-\epsilon/2}\ell_0^{\epsilon} \sim \ell_0^{\epsilon}$ in the continuous chain limit $\ell_0 \to 0$. Somewhat lengthy calculations yield the following results for the diagrams of figure 2, integrated for general d as far as possible:

$$A_1(j_1, j_2, n) = -2d\ell_0^2\beta_e^2\xi\left(\frac{d}{2}\right)\sum_{m_1=1}^{j_1-3}\sum_{m_2=j_2+1}^{n-1}(j_1 - 1 - m_1)(m_2 - m_1)^{-\frac{d}{2}-1} + \tilde{A}_1(j_1, j_2, n) \tag{A1}$$

$$\tilde{A}_1(j_1, j_2, n) = \frac{2}{d-2}\ell_0^2\beta_e^2\left\{\frac{8j_1^{2-d/2}}{d-2}[(n - j_1)^{1-d/2} - (j_2 - j_1)^{1-d/2}]\right.$$

$$+4\int_0^{j_1} \mathrm{d}x\, x^{1-d/2}\Bigg[j_1((j_2-x)^{-d/2}-(n-x)^{-d/2}) + \frac{4-d}{d-2}((j_2-x)^{1-d/2}-(n-x)^{1-d/2})\Bigg]\Bigg\} \tag{A2}$$

$$A_2(j_1, j_2, n) \equiv A_1(n-j_2, n-j_1, n) \tag{A3}$$

by reflection symmetry of the chain

$$B(j_1, j_2, n) = -2d\ell_0^2\beta_e^2\xi\left(\frac{d}{2}\right)(j_2-j_1-1)J_0 + \tilde{B}(j_1, j_2, n) \tag{A4}$$

$$\begin{aligned}\tilde{B}(j_1, j_2, n) = \frac{8}{d-2}\ell_0^2\beta_e^2\Bigg\{ & \frac{2}{d-2}(j_2-j_1)^{2-d/2}((n-j_2+j_1)^{1-d/2} \\ & -(n-j_2)^{1-d/2}-j_1^{1-d/2}) + \frac{4-d}{d-2}\frac{\Gamma^2(2-d/2)}{\Gamma(4-d)}(j_2-j_1)^{3-d} \\ & + \int_0^{j_2-j_1} \mathrm{d}x\, x^{1-d/2}[(n-x)^{1-d/2}-(n-j_1-x)^{1-d/2}-(j_2-x)^{1-d/2} \\ & -(j_2-j_1)((n-x)^{-d/2}-(n-j_1-x)^{-d/2}-(j_2-x)^{-d/2})]\Bigg\}\end{aligned} \tag{A5}$$

$$C_1(j_1, j_2, n) = -2d\ell_0^2\beta_e^2\xi\left(\frac{d}{2}\right)\sum_{m_1=3}^{j_1-1}\sum_{m_2=j_2+1}^{n-1}(m_1-1)(m_2-m_1)^{-1-d/2} + \tilde{C}_1(j_1, j_2, n) \tag{A6}$$

$$\tilde{C}_1(j_1, j_2, n) = \frac{16}{(4-d)(d-2)}\ell_0^2\beta_e^2\int_0^{j_1} \mathrm{d}x\, x^{2-d/2}[(j_2-x)^{-d/2}-(n-x)^{-d/2}] \tag{A7}$$

$$C_2(j_1, j_2, n) \equiv C_1(n-j_2, n-j_1, n) \qquad \text{by symmetry} \tag{A8}$$

$$\begin{aligned}D_1(j_1, j_2, n) \equiv \tilde{D}_1(j_1, j_2, n) = \frac{8}{d-2}\ell_0^2\beta_e^2\Bigg\{ & \frac{2}{4-d}\int_0^{j_1} \mathrm{d}x\,(n-x)^{-d/2}(j_1-x)^{2-d/2} \\ & + \int_0^{j_1} \mathrm{d}x\,\frac{1}{n-x}\int_x^{j_1} \mathrm{d}y\,[(y-x)^{1-d/2}((n-y)^{1-d/2}-(n-x)^{1-d/2}) \\ & -(y(n-x)-(y-x)^2)^{1-d/2}]\Bigg\} - (n \to j_2).\end{aligned} \tag{A9}$$

Here the contribution $(n \to j_2)$ results by replacing n by j_2 in the explicitly given contribution:

$$D_2(j_1, j_2, n) \equiv D_1(n-j_2, n-j_1, n) \qquad \text{by symmetry} \tag{A10}$$

$$\begin{aligned}E(j_1, j_2, n) \equiv \tilde{E}(j_1, j_2, n) = \frac{8}{(4-d)(d-2)}\ell_0^2\beta_e^2\Bigg\{ & d\int_0^{n-j_2+j_1} \mathrm{d}x\, x^{3-d/2}(n-x)^{-1-d/2} \\ & + d\int_{j_1}^{n-j_2+j_1} \mathrm{d}x\, x^{2-d/2}(n-x)^{-d/2}\left(1-\frac{n-j_1}{n-x}\right) \\ & + d\int_{n-j_2}^{n-j_2+j_1} \mathrm{d}x\, x^{2-d/2}(n-x)^{-d/2}\left(1-\frac{j_2}{n-x}\right) \\ & + 2\int_0^{j_1} \mathrm{d}x\, x^{2-d/2}((n-x)^{-d/2}-(j_2-x)^{-1/2}) \\ & + 2\int_0^{n-j_2} \mathrm{d}x\, x^{2-d/2}((n-x)^{-d/2}-(n-j_1-x)^{-d/2})\Bigg\}\end{aligned} \tag{A11}$$

$$F(j_1, j_2, n) \equiv \tilde{F}(j_1, j_2, n) = \frac{8}{(d-2)}\ell_0^2\beta_e^2\int_0^{j_1} \mathrm{d}x\int_0^{n-j_2} \mathrm{d}y\,\frac{1}{x+y}$$

$$\cdot\{[(y+x)(n-y-j_1+x)-x^2]^{1-d/2}-[(y+x)(n-y)-x^2]^{1-d/2}$$
$$-[(y+x)(j_2-j_1+x)-x^2]^{1-d/2}+[(y+x)j_2-x^2]^{1-d/2}\} \tag{A12}$$

$$G_1(j_1,j_2,n)\equiv\tilde{G}_1(j_1,j_2,n)=\frac{8}{d-2}\ell_0^2\beta_e^2\int_0^{j_1}\mathrm{d}x\,x$$
$$\times\left\{\int_x^{j_2-j_1+x}\frac{\mathrm{d}y}{y^2}[(n-j_1+2x-y)y-x^2]^{1-d/2}\right.$$
$$-\int_x^{j_1}\frac{\mathrm{d}y}{y^2}[(n-j_1+x)y-x^2]^{1-d/2}$$
$$+\int_{j_2-j_1+x}^{j_2}\frac{\mathrm{d}y}{y^2}[(n-j_2+x)y-x^2]^{1-d/2}$$
$$\left.-\int_{j_1}^{j_2}\frac{\mathrm{d}y}{y^2}[(n+x-y)y-x^2]^{1-d/2}\right\}-(n\to j_2) \tag{A13}$$

$$G_2(j_1,j_2,n)\equiv G_1(n-j_2,n-j_1,n)\qquad\text{by symmetry} \tag{A14}$$

$$H(j_1,j_2,n)\equiv\tilde{H}(j_1,j_2,n)=\frac{8}{d-2}\ell_0^2\beta_e^2\int_0^{j_2-j_1}\mathrm{d}x\,x$$
$$\times\left\{\int_x^{j_1+x}\frac{\mathrm{d}y}{y^2}[(n-j_1)y-x^2]^{1-d/2}-\int_{j_2-j_1}^{j_2}\frac{\mathrm{d}y}{y^2}[(n-j_2+x)y-x^2]^{1-d/2}\right.$$
$$+\int_{j_1+x}^{j_2}\frac{\mathrm{d}y}{y^2}[(n-y+x)y-x^2]^{1-d/2}$$
$$\left.-\int_x^{j_2-j_1}\frac{\mathrm{d}y}{y^2}[(n-j_1-y+x)y-x^2]^{1-d/2}\right\}-(n\to j_2). \tag{A15}$$

A.2. ϵ-expansion

Here we expand the diagrammatic contributions in powers of ϵ. The essential part of the one-loop contribution (first diagram of figure 2) is $\tilde{J}_0$, which from equations (2.19), (2.18), (2.15) is found as

$$\tilde{J}_0=\frac{4}{(4-\epsilon)(2-\epsilon)}[(\tilde{j}_2-\tilde{j}_1)^{\epsilon/2-1}+\tilde{n}^{\epsilon/2-1}-(\tilde{n}-\tilde{j}_1)^{\epsilon/2-1}-\tilde{j}_2^{\epsilon/2-1}]$$
$$=\tilde{J}_0^{(0)}+\epsilon\tilde{J}_0^{(1)}+\mathrm{O}(\epsilon^2) \tag{A16}$$

where

$$\tilde{J}_0^{(0)}=\tfrac{1}{2}[(\tilde{j}_2-\tilde{j}_1)^{-1}+\tilde{n}^{-1}-(\tilde{n}-\tilde{j}_1)^{-1}-\tilde{j}_2^{-1}] \tag{A17}$$

$$\tilde{J}_0^{(1)}=\frac{1}{4}\left[\frac{\ln(\tilde{j}_2-\tilde{j}_1)}{\tilde{j}_2-\tilde{j}_1}+\frac{\ln\tilde{n}}{\tilde{n}}-\frac{\ln(\tilde{n}-\tilde{j}_1)}{\tilde{n}-\tilde{j}_1}-\frac{\ln\tilde{j}_2}{\tilde{j}_2}\right]+\frac{3}{8}\tilde{J}_0^{(0)}. \tag{A18}$$

The two-loop diagrams are only needed up to order ϵ^0, since the renormalized coupling itself turns out to be of order ϵ. Considering $\tilde{A}_1$ (equation (A2)) with the help of equation (2.18) we find

$$\ell_0^{-4}\tilde{A}_1(j_1,j_2,n)=\frac{2}{2-\epsilon}\tilde{\beta}_e^2\left\{\frac{8\tilde{j}_1^{\epsilon/2}}{2-\epsilon}[(\tilde{n}-\tilde{j}_1)^{\epsilon/2-1}-(\tilde{j}_2-\tilde{j}_1)^{\epsilon/2-1}]\right.$$
$$\left.+4\int_0^{\tilde{j}_1}\mathrm{d}x\,x^{\epsilon/2-1}[\tilde{j}_1((\tilde{j}_2-x)^{\epsilon/2-2}-(\tilde{n}-x)^{\epsilon/2-2})\right.$$

$$+\frac{\epsilon}{2-\epsilon}((\tilde{j}_2 - x)^{\epsilon/2-1} - (\tilde{n} - x)^{\epsilon/2-1})]\Bigg\}. \tag{A19}$$

This shows a $1/\epsilon$-contribution, due to integration over small x. This easily is extracted by partial integration, with the final result

$$\ell_0^{-4}\tilde{A}_1(j_1, j_2, n) = \frac{8}{\epsilon}\tilde{\beta}_e^2\left(\frac{\tilde{j}_1}{\tilde{j}_2^2} - \frac{\tilde{j}_1}{\tilde{n}^2}\right) + 4\tilde{\beta}_e^2\Bigg[2\frac{\tilde{j}_1}{\tilde{j}_2^2}\ln\tilde{j}_2 - 2\frac{\tilde{j}_1}{\tilde{n}^2}\ln\tilde{n} + \frac{\tilde{j}_1}{\tilde{n}^2}\ln(\tilde{n} - \tilde{j}_1)$$
$$+\tilde{j}_1\ln\tilde{j}_1\left(\frac{1}{\tilde{j}_2^2} - \frac{1}{\tilde{n}^2}\right) - \frac{\tilde{j}_1}{\tilde{j}_2^2}\ln(\tilde{j}_2 - \tilde{j}_1)\Bigg]. \tag{A20}$$

In the same way we can analyse the other contributions. In fact, it turns out that to order ϵ^0 all integrals can be evaluated analytically. Since, however, the resulting expressions for the regular contributions are lengthy, here we only give the singular parts. In the final expression for the scaling function a considerable part of the regular contributions from individual diagrams cancels, and we give our full result in the main text (equations (4.3)–(4.9)).

With the singular parts made explicit, our results for the diagrammatic contributions read

$$\ell_0^{-4}\tilde{A}_2(j_1, j_2, n) = \frac{8}{\epsilon}\tilde{\beta}_e^2\left(\frac{\tilde{n} - \tilde{j}_2}{(\tilde{n} - \tilde{j}_1)^2} - \frac{\tilde{n} - \tilde{j}_2}{\tilde{n}^2}\right) + \text{regular} \tag{A21}$$

$$\ell_0^{-4}\tilde{B}(j_1, j_2, n) = \frac{8}{\epsilon}\tilde{\beta}_e^2\left[\frac{1}{\tilde{n}} - \frac{1}{\tilde{n} - \tilde{j}_1} - \frac{1}{\tilde{j}_2} - (\tilde{j}_2 - \tilde{j}_1)\left(\frac{1}{\tilde{n}^2} - \frac{1}{\tilde{j}_2} - \frac{1}{(\tilde{n} - \tilde{j}_1)^2}\right)\right] + \text{regular} \tag{A22}$$

$$\ell_0^{-4}\tilde{C}_1(j_1, j_2, n) = \frac{16}{\epsilon}\tilde{\beta}_e^2\tilde{J}_0^{(0)} + \text{regular} \tag{A23}$$

$$\ell_0^{-4}\tilde{C}_2(j_1, j_2, n) = \frac{16}{\epsilon}\tilde{\beta}_e^2\tilde{J}_0^{(0)} + \text{regular} \tag{A24}$$

$$\ell_0^{-4}\tilde{D}_1(j_1, j_2, n) = -\frac{16}{\epsilon}\tilde{\beta}_e^2\tilde{J}_0^{(0)} + \text{regular} \tag{A25}$$

$$\ell_0^{-4}\tilde{D}_2(j_1, j_2, n) = -\frac{16}{\epsilon}\tilde{\beta}_e^2\tilde{J}_0^{(0)} + \text{regular} \tag{A26}$$

$$\ell_0^{-4}\tilde{E}(j_1, j_2, n) = -\frac{16}{\epsilon}\tilde{\beta}_e^2\tilde{J}_0^{(0)} + \text{regular} \tag{A27}$$

$$\ell_0^{-4}\tilde{F}(j_1, j_2, n) = -\frac{16}{\epsilon}\tilde{\beta}_e^2\tilde{J}_0^{(0)} + \text{regular}. \tag{A28}$$

The remaining diagrams G_1, G_2, and H yield only regular contributions.

References

[1] des Cloizeaux J and Jannink G1990 *Polymers in Solution* (Oxford: Clarendon)
[2] Schäfer L 1999 *Excluded Volume Effects in Polymer Solutions* (Heidelberg: Springer)
[3] Duplantier B 1985 *J. Physique Lett.* **46** L751
[4] Schäfer L and Baumgärtner A 1986 *J. Physique* **47** 1431
[5] Domb C and Hioe F T 1969 *J. Chem. Phys.* **51** 1920
[6] Batoulis J and Kremer K 1989 *Macromolecules* **22** 4277
[7] Micka U and Kremer K 1996 *Phys. Rev.* E **54** 2653
[8] Forni A, Ganazzoli F and Vacatello M 1996 *Macromolecules* **29** 2994
[9] Miller J D 1991 *J. Stat. Phys.* **63** 89
[10] Schloms R and Dohm V 1989 *Nucl. Phys.* B **328** 639
[11] Grassberger P 1997 *Phys. Rev.* E **56** 3682

[12] Grassberger P, Sutter P and Schäfer L 1997 *J. Phys. A: Math. Gen.* **30** 7039
[13] Micka U 1997 *PhD Thesis* University of Mainz
[14] Grassberger P 1982 *Phys. Lett.* A **89** 381